Prediction of Growth-Induced Polarity in Centrosymmetric Molecular Crystals Using Force Field Methods

Claire Gervais,[†] Thomas Wüst,[†] Norwid-Rasmus Behrnd,[†] Michael Wübbenhorst,[‡] and Jürg Hulliger*,[†]

Department of Chemistry and Biochemistry, University of Berne, Freiestrasse 3, CH-3012 Berne, Switzerland, and Department of Polymer Technology, Delft University of Technology, P.O. Box 5045, NL-2600 GA Delft, The Netherlands

Received May 19, 2004. Revised Manuscript Received August 23, 2004

A three-step procedure is proposed to investigate growth-induced polarity arising in centrosymmetric crystals of dipolar molecules. It is based on (*i*) calculation of molecular interaction energies by force field methods, (*ii*) determination of the morphology, and (*iii*) use of the energies in a Markov-type growth mechanism on faces (*hkl*). Applied to *trans*-4-chloro-4′-nitrostilbene (CNS), the procedure showed that CNS crystals, although globally centric, are composed of sectors exhibiting different polar properties. The sectors related to the +*b* and −*b* directions show opposite polarity and are mainly responsible for observed second-harmonic generation and pyroelectric effects. Influence of the calculation method on the results was investigated by comparing different force fields or charges.

Introduction

Computational techniques have became in the past decades a potential alternative to experiments for investigation of single-component systems. Crystal structure[1] and morphology prediction[2] techniques, and molecular mechanics applied to crystal surfaces or to the bulk,[3] allow determination of how molecular species assemble in the solid state. Most of the studies, such as influence of the docking of impurities on surfaces,[4] simulation of twins and epitaxy,[5,6] and selective nucleation and growth of a polymorph by choosing a judicious solvent,[7,8] are investigated on the basis of a perfect periodic packing of molecules. However, besides structural defects inevitably arising in real crystals,[9] disorder of molecules[10] may sometimes lead to the invalidity of such a description for representing reality.

Here we investigate, by means of molecular modeling tools, the mechanism of creation of orientational disorder of dipolar molecules during their crystal growth, and its impact on *vectorial*, i.e., polar properties. While X-ray diffraction data may lead to classification of the system as centrosymmetric, polar effects due to a growth-induced disorder are experimentally observed.

This type of phenomenon, called *growth-induced polarity formation*, has been found in single-component crystals,[11] but also in solid solutions[12] and host−guest systems of organic molecules.[13,14] In all these studies, the dipolar molecules are described as $A - \pi - D$ (where A and D stand for acceptor and donor terminals respectively, with the dipole moment $\vec{\mu}$ pointing from A to D), a molecular architecture well-known for giving potential nonlinear optical and electronic properties.[15,16]

The mechanism of appearance of growth-induced polarity in centric crystals of dipolar molecules can be described as follows. During the growth of a face (*hkl*), 180° orientational disorder arises by docking a molecule which forms $A \cdots A$ or $D \cdots D$ interactions with its neighborhood at the surface instead of $A \cdots D$. If the probabilities of appearance of $A \cdots A$ and $D \cdots D$ are nonequal, a thermodynamic process leads to *growth-induced polarity* in the growth sector of the face (*hkl*). However, point group symmetries and particularly the center of symmetry relating different faces remain, leading thus to

* To whom correspondence should be adressed. E-mail: juerg.hulliger@iac.unibe.ch.
† University of Berne.
‡ Delft University of Technology.

(1) Sam Motherwell, W. D.; Ammon, H. L.; Dunitz, J. D.; Dzyabchenko, A.; Erk, P.; Gavezzotti, A.; Hofmann, D. W. M.; Leusen, F. J. J.; Lommerse, J. P. M.; Mooij, W. T. M.; Price, S. L.; Scheraga, H.; Schweizer, B.; Schmidt, M. U.; van Eijck, B. P.; Verwer, P.; Williams, D. E. *Acta Crystallogr. B* **2002**, *58*, 647−661.
(2) Bisker-Leib, V.; Doherty, M. F. *Cryst. Growth Des.* **2003**, *3*, 221−237, and references therein.
(3) Myerson, A. S. *Molecular Modeling Applications in Crystallization*; Cambridge University Press: New York, 1999.
(4) Myerson, A. S.; Jang, S. M. *J. Cryst. Growth* **1995**, *156*, 459−466.
(5) Fleming, S. D.; Parkinson, G. M.; Rohl, A. L. *J. Cryst. Growth* **1997**, *178*, 402−409.
(6) Gervais, C.; Beilles, S.; Cardinaël, P.; Petit, S.; Coquerel, G. *J. Phys. Chem. B* **2002**, *106*, 646−652.
(7) Blagden, N.; Cross, W. I.; Davey, R. J.; Broderick, M.; Pritchard, R. G.; Roberts, R. J.; Rowe, R. C. *Phys. Chem. Chem. Phys.* **2001**, *3*, 3819−3825.
(8) Cross, W. I.; Blagden, N.; Davey, R. J.; Pritchard, R. G.; Neumann, M. A.; Roberts, R. J.; Rowe, R. C. *Cryst. Growth. Des.* **2003**, *3*, 151−158.
(9) Klapper, H. *Mater. Sci. Forum* **1998**, *276−277*, 291−306.
(10) Harada, J.; Ogawa, K. *J. Am. Chem. Soc.* **2001**, *123*, 10884−10888.
(11) Kluge, S.; Budde, F.; Dohnke, I.; Rechsteiner, P.; Hulliger, J. *Appl. Phys. Lett.* **2002**, *81*, 247−249.
(12) Kluge, S.; Dohnke, I.; Budde, F.; Hulliger, J. *CrystEngComm* **2003**, 67−69.
(13) Hulliger, J. *Chimia* **2001**, *55*, 554−561.
(14) Hulliger, J.; König, O.; Hoss, R. *Adv. Mater.* **1995**, *7*, 719−721.
(15) Zyss, J.; Nicoud, J. F. *Curr. Op. Solid State Sci.* **1996**, *1*, 533−546.
(16) Pan, F.; Bosshard, C.; Wong, M. S.; Serbutoviez, C.; Schenk, K.; Gramlich, V.; Günter, P. *Chem. Mater.* **1997**, *9*, 1328−1334.
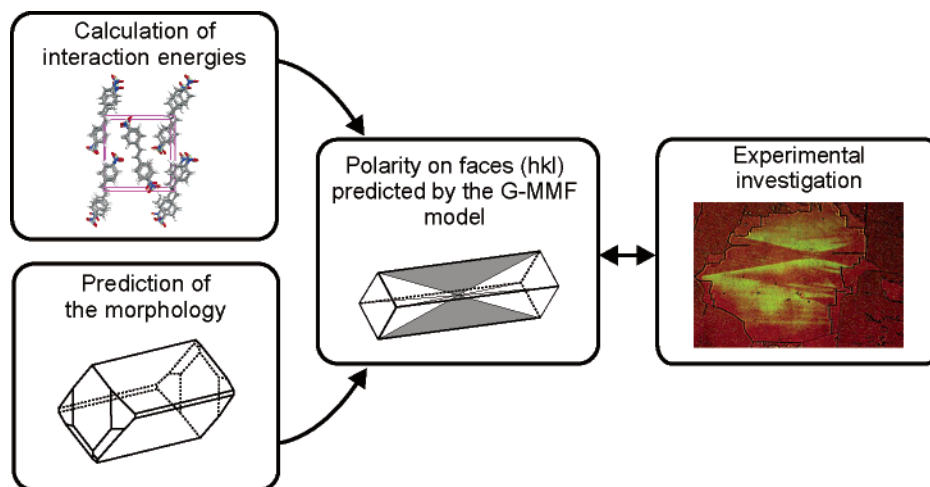
Figure 1. Methodology applied to analyze growth-induced polarity formation in a "centric" crystal of *trans*-4-chloro-4′-nitrostilbene (CNS).

a globally centric crystal object (if growth is equally fast for symmetry related sectors). Therefore, determination of the crystal structure by single-crystal X-ray diffraction may find a centric space group or 180° "twinning", while physical analyses show second-harmonic generation (SHG) or pyroelectric effects in some sectors of the crystal.

So far, polarity formation in single-component organic crystals has been theoretically studied by means of a Markov-mean field (MMF) model and Monte Carlo simulations.[17,18] In these studies, polarity formation is expressed by the states *down* ($\downarrow$) and *up* ($\uparrow$) of the projection of the molecular dipole moment along the growth axis of faces (*hkl*). In a perfectly centrosymmetric structure, the molar fraction $X(\downarrow)$ is equal to $X(\uparrow)$. Polarity arises if $X_{net} = X(\downarrow) - X(\uparrow)$ ($-1 \leq X_{net} \leq 1$) differs from zero. Physical properties having their origin in polar properties of the molecules may be described as being proportional to X_{net}. These calculations were restricted on *assumed* interaction energies for a square lattice so that results were limited to descriptive considerations.

In this paper, we theoretically investigate (in comparison to key experiments) a real system in which interaction energies are explicitly calculated and the specific symmetry of the lattice is taken into account. The chosen dipolar molecule is *trans*-4-chloro-4′-nitrostilbene (CNS hereafter), which crystallizes in a centric space group but shows a significant SHG effect[11] and a spatially inhomogeneous pyroelectric response.

The following three-step procedure is proposed for studying theoretically the polarity in CNS (Figure 1): (*i*) force field calculation of the molecular interaction energies, (*ii*) theoretical and experimental determination of the morphology of CNS crystals, and (*iii*) application of a generalized Markov mean-field model (GMMF) to the most prominent faces (*hkl*). Interpretation of the theoretical results and comparison with experimental data are discussed. Possible improvements of the procedure in view of its generalization and influence of other factors on growth-induced polarity are considered.

1. Analysis of Interactions in the CNS Crystal Structure

1.1 Crystal Packing of CNS. According to the crystallographic analysis in ref 11, CNS crystallizes in space group $P2_1/c$ (2/m), with $a = 3.836$ Å, $b = 12.916$ Å, $c = 12.221$ Å, $\beta = 93.91°$. Molecules are nearly planar, whereas in the gas phase ab initio quantum mechanical calculations provide a torsion angle of $\sim 20°$. The dipole moment of CNS is aligned close to the direction $|NO_2 - Cl|$ and forms an angle θ of about 18° to the [010] direction. Molecules are positioned on the center of symmetry leading to an occupancy of 50%:50% *on average* for $A(NO_2)$ and $D(Cl)$ terminal groups (Figure 2, left). However, as described later on, a reinvestigation by X-ray diffraction of single crystals grown from toluene led to a distribution 60%:40% and space group $P1$.

Concerning tensorial properties, $\theta = 18°$ implies that main effects of e.g., second-order optical nonlinearity or pyroelectricity is expected to be observed in the direction of the b axis. Indeed, polarized second-harmonic microscopy performed on c-plate CNS crystals obtained from the melt has shown a maximum of $2w$ light for the $\pm b$-sectors. Moreover, phase-sensitive second-harmonic microscopy (PS-SHM)[19] and scanning pyroelectric microscopy (SPEM),[20] two experimental techniques developed for studying growth-induced polarity, could demonstrate opposite signs for the polarization in $+b$ and $-b$ sectors (see ref 11 and figures in the discussion). So far, PS-SHM and SPEM did not provide an absolute value or a sign for the net polarization.

To compare with experimental results, the states *up* and *down* of the molecules are defined hereafter by the projection of their dipole moment along the $+b$ axis (Figure 2, right).

1.2 Calculation of Molecular Interaction Energies. The relevant molecular interaction energies driving polarity formation are identified as follows. (*i*) Neighbors showing significant interaction energies with a reference molecule are selected. By calculating the effect that additional neighbors

(17) Hulliger, J.; Bebie, H.; Kluge, S.; Quintel, A. *Chem. Mater.* **2002**, *14*, 1523−1529.

(18) Bebie, H.; Hulliger, J.; Eugster, S.; Alaga-Bogdanović, M. *Phys. Rev. E* **2002**, *66*, 021605.

(19) Rechsteiner, P.; Hulliger, J.; Flörsheimer, M. *Chem. Mater* **2000**, *12*, 3296−3300.

(20) Quintel, A.; Hulliger, J.; Wübbenhorst, M. *J. Phys. Chem. B* **1998**, *102*, 4277−4283.

Polarity in Centrosymmetric Molecular Crystals

Chem. Mater., Vol. 17, No. 1, 2005   87
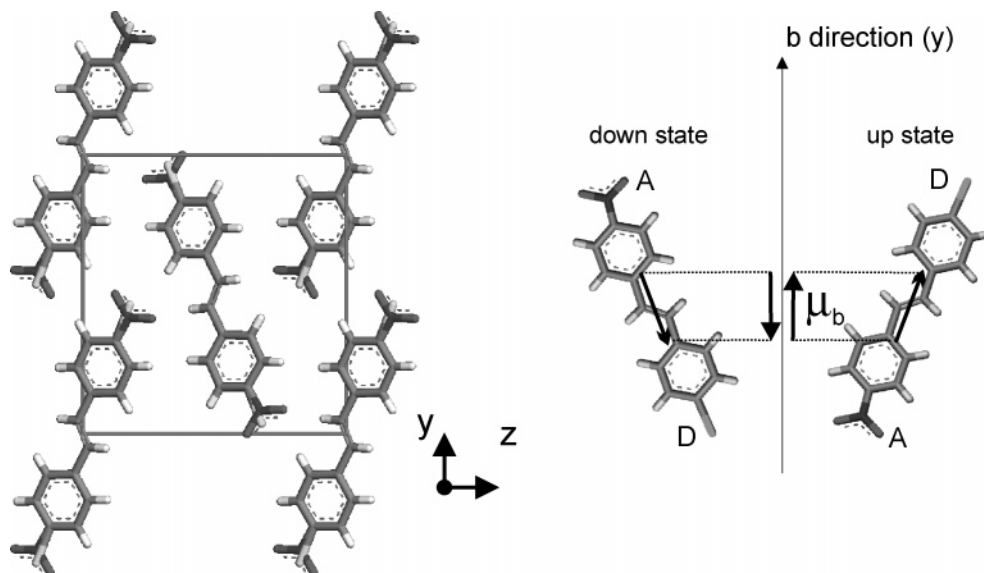
Figure 2. Left: Crystal structure of CNS showing the 180° orientational disorder of the molecules around the symmetry center. Right: the two possible states of the molecules *up* and *down* are defined by taking into account the projection of the dipole moment along the *b* axis (μ_b). Projections of μ onto the axes *a* and *c* are not taken into account.

have on the value of X_{net}, it was found that the first nearest neighbors are sufficient to give a good description of the polar properties of the system. (*ii*) All the possible interaction energies between the reference molecule and its neighbors in the bulk are calculated. Energies E_{rn}^{i} are defined, where *r* denotes the state *up* (*u*) or *down* (*d*) of the reference molecule, *n* denotes the state *up* (*u*) or *down* (*d*) of the neighbor molecule, and *i* labels the type of the neighbor (see Figure 3). For instance, E_{du}^{L3} represents the interaction energy between the reference molecule in state *down* (*d*) and the neighbor *L3* in state *up* (*u*).

A molecule is surrounded in the bulk by $\lambda_T = 20$ nearest neighbors, classified according to their type of contact with the reference molecule (Figure 3): tip-back contacts between *Cl* and *NO$_2$* groups, side contacts between aromatic moieties, or mixed contacts involving a *Cl* or *NO$_2$* group and the *C*-frame of the molecules.

There is a total of 80 interaction energies to be calculated ($2 \times 2 \times \lambda_T$, according to the *up* and *down* states of both reference and neighbor molecules). However, the center of symmetry induces a correspondence between the energy values of the interactions of the same type (*tip-back*, *side*, or *mixed*):

$$E_{dd}^{i} = E_{uu}^{j}, \qquad (1)$$

$$E_{ud}^{i} = E_{du}^{j}, \qquad (2)$$

with $[i, j]$ = [B1,U3], [B2,U2], [B3,U1], [U1,B3], [U2,B2], [U3,B1], [L1,R3], [L2,R2], [L3,R1], [R1,L3], [R2,L2], [R3,L1], [Lu1,Ru3], [Lu2, Ru2], [Lu3,Ru1], [Ru1,Lu3], [Ru2,Lu2], [Ru3,Lu1], [N1,N2], [N2,N1].

Starting with a supercell $a \times b \times c = 6 \times 3 \times 3$, we calculated E_{dd}^{i} and E_{ud}^{i}[21] and deduced E_{uu}^{j} and E_{du}^{j} from eqs 1 and 2. The supercell was established and energies were calculated by using the modules Visualizer and Discover of the software package Materials Studio from Accelrys Inc.[22]

We used the consistent force field Compass[23] with group-based cutoff (groups defined as the entire molecules) for both Coulombic and van der Waals interactions. A cutoff distance of 60 Å (with spline width 20 Å, buffer width 8 Å, and vdW tail correction 60 Å) was chosen to ensure the correctness of the energies.[24] Influence of the optimization of the structure was studied by calculating energies in three different ways: (*i*) no minimization of the supercell, (*ii*) partial minimization, where only the reference molecule is allowed to relax, and (*iii*) full minimization, both intermolecular and intramolecular parameters of all the molecules are optimized. Whatever the method, the lattice was kept fixed to avoid an artificial variation of the energies due to a deviation of the cell parameters from their original values.[25] As shown in the Supporting Information, the three methods give similar energy values. For results hereafter, atomic coordinates determined by X-ray analysis were conserved and no minimization of the supercell was performed. The total set

(21) The procedure consisted of the following: Construction of a supercell $a \times b \times c = 6 \times 3 \times 3$ with all the CNS molecules in *down* state and calculation of energies E_{dd}^{i}. Then, rotation by 180° (to be in *up* state) of one molecule located in the middle of the supercell (reference molecule) and calculation of energies E_{ud}^{i}.

(22) Accelrys Inc. *Materials Studio, Release 3.0*; Accelrys Inc.: San Diego, CA, 2003.

(23) Sun, H. *J. Phys. Chem. B* **1998**, *102*, 7338−7364. *Compass 1.0. Condensed phase Optimized Molecular Potentials for Atomistic Simulation Studies*; Distributed by Accelrys Inc.: San Diego, CA.

(24) Indeed, a cutoff distance below 30 Å would lead to incomplete values for *tip-back* interactions since in this type of dimers the distance between the furthest atoms of two adjacent molecules (or groups) is about 30−35 Å (molecular length ≈ 15 Å). See Supporting Information for a graph showing the variation of the energies according to the cutoff distance.

(25) Results of the full optimization (including cell parameters) of supercells containing various ratios of *up* and *down* molecules randomly distributed are shown in Supporting Information. A deviation of the cell parameter *a* and the angle β is observed in all the structures. However, its intensity is proportional to the ratio and varies with the spatial distribution of *up* and *down* molecules. Therefore, optimizing the supercells with all the molecules *down* (for calculation of E_{dd}) and with a reference *up* surrounded by *down* molecules (for calculating E_{ud}) would lead to different deviations of the crystal packings for the two structures, and thus to a supplementary source of error.
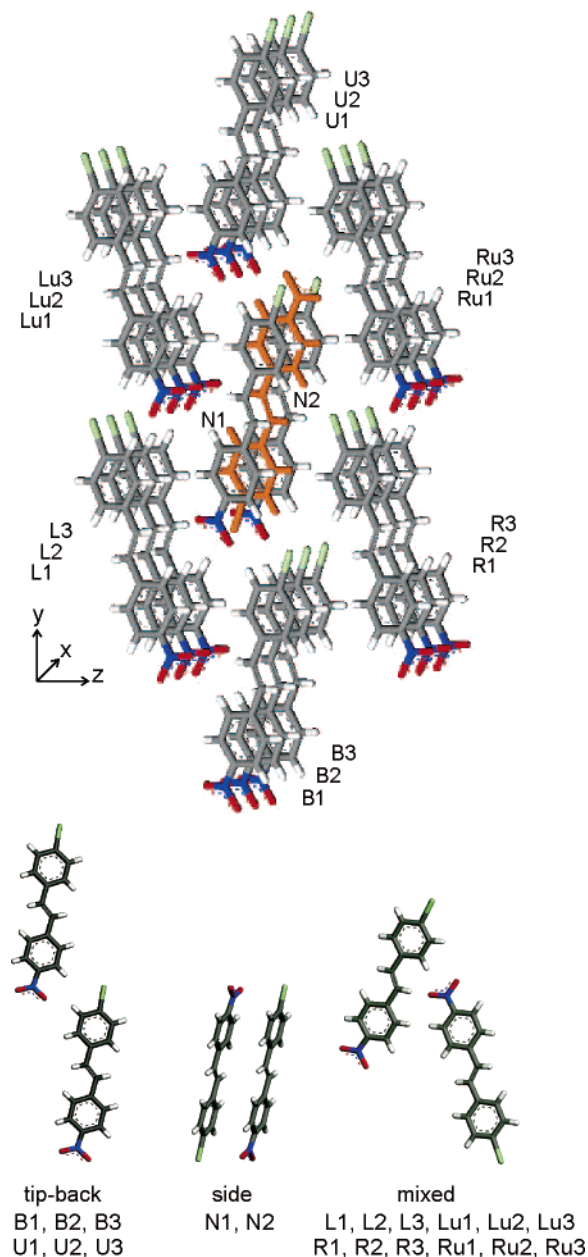
Figure 3. Top: Neighborhood of a reference molecule (orange) in the bulk. The 20 neighbors are designated by labels giving their position relative to the reference molecule. Here, the reference molecule is in state *down* and is surrounded by neighbors in state *up*, so that all the energies are denoted E_{du}^i, with i label of the neighbor considered. Bottom: Classification of the neighbors according to their type of contacts with the reference molecule.

Table 1. Interaction Energies [kJ/mol] between a Reference Molecule and Its 20 Nearest Neighbors in the Bulk[a]

i	E_{dd}^i	E_{ud}^i	E_{du}^i	E_{uu}^i
B1	−1.07	−1.77	−0.72	−1.07
B2	−5.45	−8.94	−3.92	−5.45
B3	−4.45	−7.92	−3.74	−4.45
U1	−4.45	−3.74	−7.92	−4.45
U2	−5.45	−3.92	−8.94	−5.45
U3	−1.07	−0.72	−1.77	−1.07
N1	−19.44	−21.93	−22.48	−19.44
N2	−19.44	−22.48	−21.93	−19.44
L1	−1.78	−1.60	−1.62	−1.67
L2	−6.08	−4.73	−6.37	−5.30
L3	−3.58	−7.11	−3.87	−7.58
Lu1	−1.78	−1.62	−1.60	−1.67
Lu2	−6.08	−6.37	−4.73	−5.30
Lu3	−3.58	−3.87	−7.11	−7.58
R1	−7.58	−7.11	−3.87	−3.58
R2	−5.30	−4.73	−6.37	−6.08
R3	−1.67	−1.60	−1.62	−1.78
Ru1	−7.58	−3.87	−7.11	−3.58
Ru2	−5.30	−6.37	−4.73	−6.08
Ru3	−1.67	−1.62	−1.60	−1.78

[a] The neighbors are gathered according to their type of contact with the reference molecule (*tip-back, side, mixed*) to highlight the center of symmetry relating the energy values (see eqs 1 and 2). For notation of the neighbors and of the energies, see Figure 3 and text.

1.3 Determination of the Crystal Morphology. Crystals were grown by slowly decreasing the temperature (from 90 to 25 °C within 2−3 days) of a solution of CNS in dimethylformamide (DMF). The crystals exhibited a long needle shape with a distinct rhombic section. By performing goniometric measurements on several representative crystals and by indexing the faces of a crystal mounted on an X-ray diffractometer, the following conclusions could be drawn. (*i*) The four predominant faces belong to the family {011}. (*ii*) It is likely that each extremity is composed of one single face belonging to {n00}. Crystals grown from less polar solvents such as ethanol or from vacuum exhibited similar shapes, indicating that the polarity of the solvent does not have a strong effect on the morphology.

To complement these results, the morphology was calculated by using computational tools. Prediction methods taking into account energy calculations[2] are difficult to apply here because of the orientational disorder. Therefore, we restrained ourselves to the Bravais−Friedel−Donnay−Harker (BFDH) method[27] based on purely geometrical considerations: the larger the interplanar spacing, the more predominant the face. The calculated morphology is in agreement with the experimental one, showing predominant faces {011} and {100}, see Figure 4.

Therefore, we have investigated polarity formation arising during the growth of the following family of faces: {011}, {100}, and {110}. Although it is likely that {110} faces do not appear in real crystals, they were studied for comparison.

1.4 Structural and Energetical Analysis Involving Different Faces. As shown in Figure 5, a reduction of symmetry is observed for the three faces (011), (110), and (100). Consequently, two sites *A* and *B* have to be considered at the surfaces: for (011) and (110), all point symmetry elements are lost leading to a 2D symmetry *p*1, so that *A* and *B* sites are symmetry independent. For (100), the 2-fold

of energies presented in Table 1 highlights the spatial distribution of energies in the neighborhood. This anisotropy has no consequence in the bulk but *becomes fundamental for attaching molecules to faces*. On a growing surface (*hkl*) composed of only a subset {*i*} of the 20 neighbors, a breaking of symmetry with respect to the energies ($E_{ud}^i(hkl) \neq E_{du}^i(hkl)$ or $E_{dd}^i(hkl) \neq E_{uu}^i(hkl)$) may appear and can lead to polarity properties such as a pyroelectricity or SHG effect that would be forbidden in the bulk.[26] To recognize the most important faces on CNS crystals, the morphology was determined both experimentally and theoretically.

(26) Zyss, J.; Oudar, J. L. *Phys. Rev. A* **1982**, *26*, 2028−2048.

(27) Donnay, J. D. H.; Harker, D. *Am. Mineral.* **1937**, *22*, 446−467.

Polarity in Centrosymmetric Molecular Crystals

Chem. Mater., Vol. 17, No. 1, 2005 89
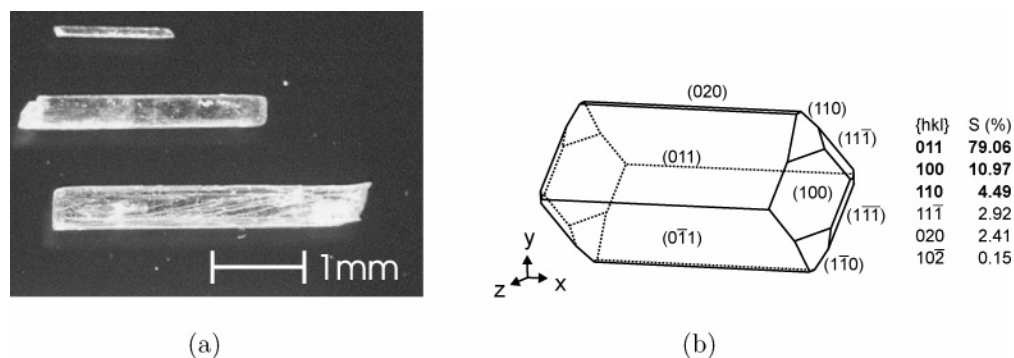
Figure 4. (a) Morphology of CNS crystals grown in DMF. (b) Theoretical investigation on the morphology of CNS crystals by using the BFDH model. b) left: Prediction of the crystal shape. For more clarity, only visible faces are labeled. b) right: Surface area (S) of the visible faces (*hkl*). Selected faces are in bold.
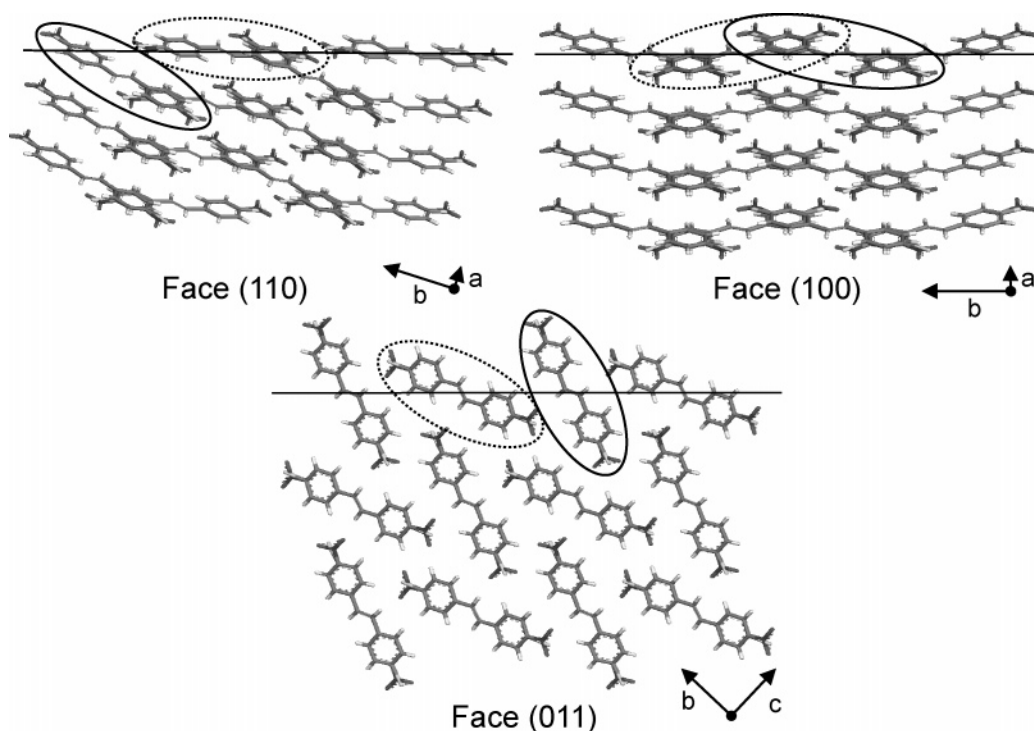
Figure 5. Illustration of the most important faces of CNS crystals. Ellipsoids indicate the two sites *A* (solid) and *B* (dashed) emerging on surfaces.

Table 2. Neighborhood of the Different Faces Investigated[a]

face (*hkl*)	λ	site	neighborhood {*i*}
011	14	A	B1 B2 B3 L1 L2 L3 Lu1 Lu2 Lu3 R1 R2 R3 N1 N2
		B	B1 B2 B3 L1 L2 L3 Ru1 Ru2 Ru3 R1 R2 R3 N1 N2
100	13	A	B1 L1 Lu1 R1 Ru1 U1 N1 B2 L2 Lu2 R2 Ru2 U2
		B	B3 L3 Lu3 R3 Ru3 U3 N2 B2 L2 Lu2 R2 Ru2 U2
110	12	A	B1 B2 B3 L1 L2 R1 R2 N1 L3 R3 Lu1 Ru1
		B	B1 B2 B3 L2 L3 R2 R3 N2 L1 R1 Lu3 Ru3

[a] Notations are given in Figure 3. For other faces of the three families ({011}, {100}, and {110}), see Supporting Information.

screw symmetry is broken, leading to a 2D symmetry *pg*[28] and symmetry dependent sites *A* and *B* (eqs 1 and 2 relate the two sites). The neighborhood for sites *A* and *B* of the three faces are collected in Table 2.

On a face (*hkl*), considering a neighborhood {*i*} (see Table 2) composed of *X up* and (λ − *X*) *down* molecules, we may define a difference of energy when docking a reference molecule *down* or *up* by summing over λ, i.e., all the pairwise

(28) Weissbuch, I.; Addadi, L.; Lahav, M.; Leiserowitz, L. *Science* **1991**, *253*, 637−645.

interaction energy differences. Taking into account all the possible configurations (*n*) for a given *X*, the average total energy difference is

$$\langle \Delta E_{\text{config}} \rangle = \frac{1}{C} \sum_{n=1}^{C} \left[\sum_{\{i|up\}_n} (E_{du}^{i} - E_{uu}^{i}) + \sum_{\{i|down\}_n} (E_{dd}^{i} - E_{ud}^{i}) \right], \text{ with } C = \frac{\lambda!}{(\lambda - X)!} \quad (3)$$

{*i|up*}$_n$ and {*i|down*}$_n$ are the two subsets of a neighborhood {*i*} with configuration *n*, being composed of *X* neighbors in state *up* and (λ − *X*) neighbors in state *down*, respectively. We define by $\langle \Delta E_{\text{config}} \rangle_A$ and $\langle \Delta E_{\text{config}} \rangle_B$ the average total energy differences for site *A* and site *B*, respectively.

By looking at the variation according to *X* of $\langle \Delta E_{\text{config}} \rangle_{A+B}$ = $\langle \Delta E_{\text{config}} \rangle_A$ + $\langle \Delta E_{\text{config}} \rangle_B$, indications about the polar behavior of the faces can be obtained (Figure 6) as follows. (1) For faces (011) and (110), $\langle \Delta E_{\text{config}} \rangle_{A+B}$ values are mainly positive (Figure 6c and a, respectively). Considering eq 3, it means that whatever *X* is the system has a tendency to have

(a) Face (110)

(b) Face (100)

(c) Face (011)

Figure 6. Investigation of the energy differences $\langle \Delta E_{config} \rangle$ resulting from the docking of a molecule in a neighborhood composed of X molecules in state *up* and $(\lambda - X)$ in state *down*. Possible errors arising from the calculation of interaction energies are taken into account by varying the energies $\pm 5\%$ in eq 3.

a higher probability to dock molecules in state *up*, i.e., with μ_b parallel to the $+b$ direction (see Figure 2). As shown in Figure 5, the corresponding surfaces are composed mostly of *Cl* groups pointing toward the nutrient. (2) As expected, the face (100) reflects symmetry between the energies of the two sites *A* and *B*, leading to $\langle \Delta E_{config} \rangle_{A+B} = 0$ for a neighborhood composed of 50% of *up* and 50% *down* molecules (see Figure 6b). Corresponding sectors should therefore develop no polarity.

This configurational study highlights a relationship between symmetry of a surface and growth-induced polarity and gives already a strong argument for the direction of polarity at different faces.

To calculate values for $X_{net} = X(\downarrow) - X(\uparrow)$, a modified version of the Markov-mean-field model was set up. Agreement with points (1) and (2) should be obtained for X_{net} values, i.e., *negative* for faces (011) and (110) and *zero* for face (100). Moreover, considering that $\langle \Delta E_{config} \rangle$ for (110) is always positive which is not the case for (011), one may expect $| X_{net}(110)| > | X_{net}(011)|$.

2. Markov Model of Polarity Formation

2.1 Overview of Theoretical Models Used Previously. Theoretical investigation of polarity formation arising on a face (*hkl*) is based on the following growth model. (*i*) The face (*hkl*) is described as a stacking of layers composed of dipolar molecules. The orientational state of molecules is viewed by the projection of the dipole moment onto the growth direction (states: *up* and *down*). (*ii*) A layer-by-layer growth on the face is represented as a succession of steps, consisting of attachment of a complete new layer (called the

adlayer), and thermal relaxation of the adlayer with respect to *up* and *down* states, while the former layers are kept frozen.

The lattice is defined as quadratic, where a molecule on a surface site is surrounded by four nearest neighbors within the same layer (lateral) and one nearest neighbor located on the corresponding site of the previous layer (longitudinal).

Growth-induced polarity formation as introduced above can be described analytically by a Markov process. In such a stochastic process, the evolution of a system is fully determined by taking into account the following: (*i*) the ratio *up*/*down* of molecules in the previous layer, and (*ii*) transition probabilities, which are given by probabilities of attaching a molecule with a given orientation (*up* or *down*) onto a molecule of the previous layer. These probabilities are directly related to the interaction energies involved in the attachment. To take into account the influence of the four nearest neighbors within the same layer, a mean-field correction was introduced (average among all the lateral interaction energies weighted by the ratio *up*/*down*) and included in the transition probabilities (Figure 7, left). The Markov mean-field model (MMF) already showed its capability to depict the possible behavior of a system in terms of polarity.[17,18]

2.2 Generalized Markov Mean-Field Model: Application to CNS. Although the MMF model is satisfactory to investigate theoretically the main features responsible for polarity formation of single-component molecular crystals, it becomes inadequate for the analysis of a structure such as CNS. Two main difficulties are highlighted. First, as shown in Figure 3, surfaces may exhibit crystallographically dif-
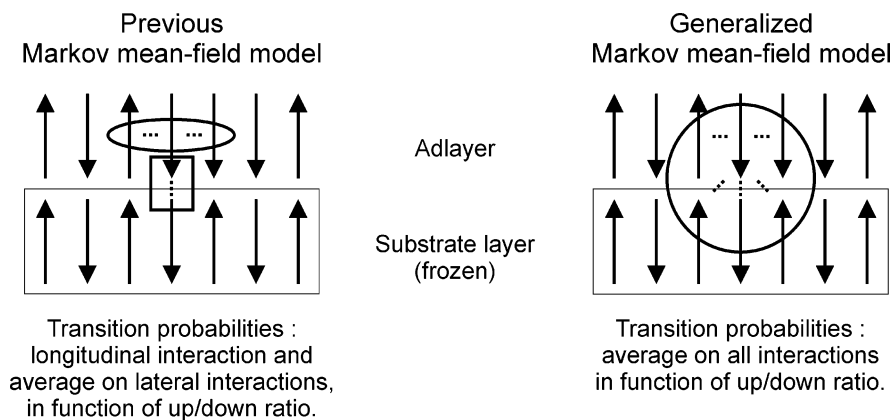
Figure 7. Basic principle of the Markov mean-field model (MMF)[17,18] used for theoretical investigations of single-component molecular crystals (left) and the generalized mean-field model (GMMF) adapted for the analysis of CNS (right). Circled areas: mean-field averaging.

ferent sites, each reflecting a distinct neighborhood, so that the use of a single set of transition probabilities is no longer sufficient. The two sites are represented by separate Markov chains using different transition probabilities arising from neighborhood *A* and *B*. Second, the presence of several *longitudinal* neighbors leads to the impossibility to make a quantitative prediction of X_{net}. Consider the transition probability P_{du} defined as the probability to attach a molecule *down* onto a molecule *up* of the previous layer. In the presence of several longitudinal neighbors, this leads to a probability defining the attachment of a molecule *down* onto molecules being *all up* in the previous layer. In that case, all the configurations showing *a mixture of the two states* in the longitudinal neighborhood conceptually impede a consistent description.

To overcome this difficulty, the MMF model is modified in the following way. The notion of lateral and longitudinal neighbors is discarded and replaced by a *mean-field applied to all the neighbors*, i.e., the transition probabilities are defined as the probability to attach a molecule in state *up* or *down* in a given environment (Figure 7, right).

2.3 Application to Faces (011), (110), and (100). Because point group symmetries are present between the different growth sectors of a family {*hkl*} (see Section 1.4), it is sufficient to calculate X_{net} for one face (*hkl*) only. Indeed, the symmetry center, the 2-fold axis, and the symmetry plane normal to *b*, respectively, lead to the following:

$$X_{net}(hkl) = -X_{net}(\bar{h}\bar{k}\bar{l}), \tag{4}$$

$$X_{net}(hkl) = +X_{net}(\bar{h}k\bar{l}), \tag{5}$$

$$X_{net}(hkl) = -X_{net}(h\bar{k}l). \tag{6}$$

Considering the sign of X_{net}, it defines the predominant terminal group (*Cl* or *NO_2*) appearing at the surface of a face, but also at surfaces of all the other faces of a family. Indeed, one has to keep in mind that X_{net} is defined by the difference in the population of molecules being in *down* and *up* states *according to the +b axis*, so that eqs 4–6 refer to the same relative orientation of the molecules with respect to the growth directions of the faces.

For the purpose of a comparison, X_{net} values were calculated by using the set of energies given in Table 1.

Table 3. X_{Net} Calculated by Using the GMMF Model and Energies Computed with Different Force Fields[a]

method	face (110)	face (100)	face (011)
Compass	−0.49 ± 0.02	−0.01 ± 0.01	−0.47 ± 0.02
Dreiding-gast	−0.56 ± 0.05	−0.01 ± 0.05	−0.45 ± 0.11
Dreiding-cheq	−0.64 ± 0.12	−0.01 ± 0.07	−0.58 ± 0.17
Universal-gast	−0.76 ± 0.02	+0.04 ± 0.02	−0.73 ± 0.02

[a] Errors attributed to individual energies are set to ± 10%. Consistent with symmetry, $X_{net}(100)$ gives exactly zero if no error is assigned to the energies. Note that the sign of X_{net} is not affected by varying force fields or charges.

Energies obtained by the Dreiding 2.21[29] and the Universal[30] force fields with different charge sets (Gasteiger and charge equilibration) were used as well. Implemented charges are not really performant but may give a preliminary estimate for the sensitivity of the generalized Markov mean-field model to force fields. Similarly to the configurational study, here errors within ±10% were allowed for individual energies.

Summarized in Table 3, X_{net} values for faces (110), (100), and (011) confirm the predictions made previously (Section 1.4), i.e., $X_{net}(100) = 0$ and $X_{net}(110) \leq X_{net}(011) < 0$. A *negative* value of X_{net} for face (011) implies that surfaces of all faces {011} are composed mainly of *up* molecules, i.e., with *Cl* groups pointing predominantly toward the nutrient.

3. Discussion

3.1 Sensitivity of the Markov Model to Force Fields. Whereas the application of ±10% of errors on energies does not have a large influence on results (e.g., error on the second digit for compass) the force field method used to calculate them seems to have a significant impact on X_{net} values. On the other hand, converted to the percentage of *up* molecules located on the surfaces, we obtain to some extent narrow ranges: 74.5–88.0% for face (110) and 72.5–86.5% for face (011).

Considering the disparity observed for the absolute energies (see Supporting Information), the homogeneity between the different force fields may be at first glance surprising.

(29) Mayo, S. L.; Olafson, B. D.; Goddard, W. A. *J. Chem. Phys.* **1990**, *94*, 8897–8909.
(30) Rappe, A. K.; Casewit, C. J.; Colwell, K. S.; Goddard, W. A.; Skiff, W. M. *J. Am. Chem. Soc.* **1992**, *114*, 10024–10035.
(31) Hulliger, J. *Encyclopedia of Supramolecular Chemistry*; Marcel Dekker: New York, 2004; pp 1120–1128.
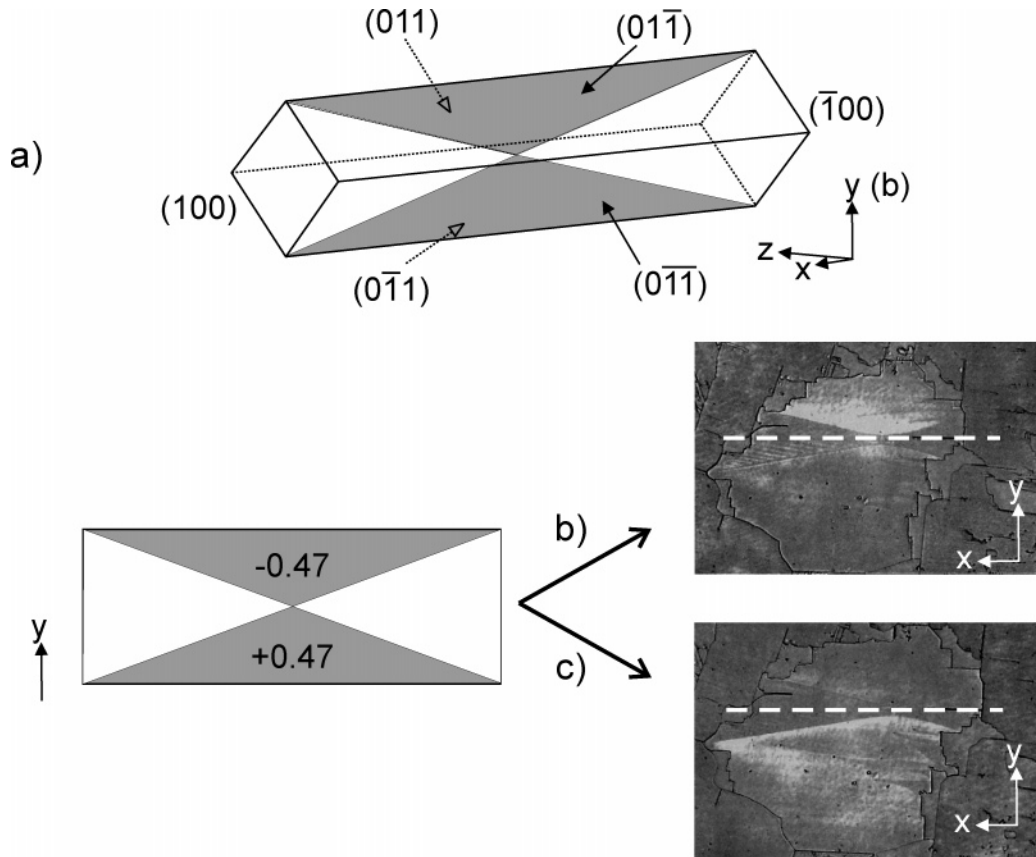
Figure 8. Polarity behavior expected by the generalized Markov mean-field model and comparison with experimental data. (a) Representation of the cone-shaped distribution of polarity derived from GMMF results (grey, sectors showing polarity; white, no polarity expected). (b) and (c) Good agreement between polar effects calculated for different regions (left) and SHG measurements performed by PHSHM on millimeter-sized CNS crystals (right).[31] For SHG measurements, the polarization of the fundamental wave (1064 nm) is parallel to the *b* axis revealing an effect of contrast for the *upper b*-sector (b) and for the *lower b*-sector (c).

However, the GMMF model is determined only by *energy differences*, so that a basic bias due to an inadequate force field or set of charges (leading to high errors on absolute energies) is canceled out in the calculation of X_{net}. Moreover, the high number of energy values taken into account here and their average by a mean-field correction reduces the total error of X_{net}.

3.2 Comparison with Experimental Data. Assuming that nucleation occurred at the center of a crystal, one may represent the repartition of polarity in the entire crystal volume as shown Figure 8a: four {011} growth sectors, in which *Cl* groups are predominantly pointing toward the nutrient, and two {100} cone-shaped sectors exhibiting no polarity.

For comparison with experimental data, one has to keep in mind that measured polarity depends on the type of the experimental approach (measured for a surface or the bulk, at what spatial resolution, in which direction within the crystal, etc.). We will restrict our study to two experimental tools developed particularly for growth-induced polarity, i.e., phase-sensitive second-harmonic microscopy (PH-SHM) and scanning pyroelectric microscopy (SPEM).[13]

In reference 11, PH-SHM was applied to 20 CNS plate crystals with (001) orientation, which were grown by different attempts from the melt. Three main observations were done: (*i*) the optical nonlinearity was predominantly observed in the *b* direction, (*ii*) polarization in +*b* and −*b* directions differed in the sign of polarity, and (*iii*) no

significant polarity was observed along the *a* axis. Because X_{net} values calculated here correspond to the difference *down* vs. *up* of the projection of the dipole moment along *b*, comparison can be done only with experimental results obtained along this direction, that is (*i*) and (*ii*).

Regions observed on crystals (see Figure 8a) can be composed of superimposed growth sectors, so that a polar effect ($\mathscr{P}_R$, vector property) of a region may be defined by

$$\mathscr{P}_R = \sum_i \frac{V^i}{V^R} X_{net}^i \tag{7}$$

with volume V^i and X_{net}^i defined for each growth sector *i* present in the region *R* of volume V^R. Physical properties related to polarity are assumed here to be proportional to $\mathscr{P}_R$.

Crystals in the (*a*, *b*) plane show four distinct regions, named *upper*, *lower*, *left*, and *right* according to their location in Figure 8. The *upper* and *lower* parts are a combination of the growth sectors of [(011) + (01$\bar{1}$)] and [(0$\bar{1}$1) + (0$\bar{1}\bar{1}$)], respectively. In each case, the volumes and the X_{net} values of the two growth sectors are the same, leading to $\mathscr{P}_{upper} = -0.47$ and $\mathscr{P}_{lower} = +0.47$ (opposite sign because of a description within a common coordinate system along +*b*). *Left* and *right* parts are composed of {100} growth sectors, leading to $\mathscr{P}_{right} = \mathscr{P}_{left} = 0$.

These data are in qualitative agreement with experimental PH-SHM measurements, because (*i*) highest polar effects are
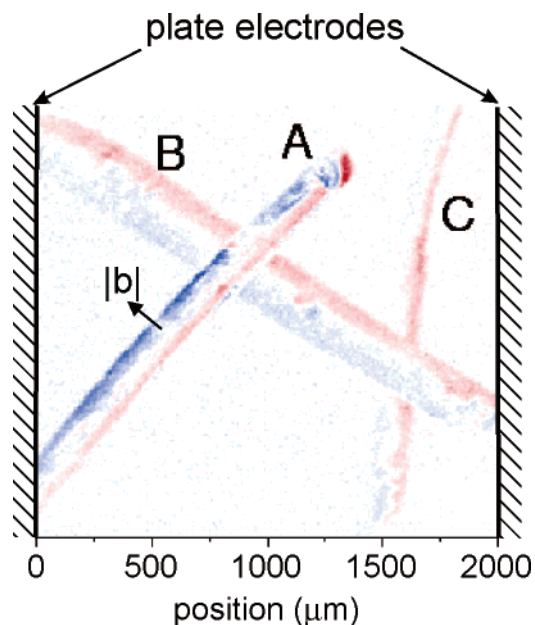
Figure 9. Pyroelectric measurements performed by SPM at 408 K. The three crystals (A, B, and C) of CNS show a bipolar state: one side is blue, the other side is red to indicate the opposite sign of polarity. Note that the sign of b is not determined.

encountered along the *b* axis, and (*ii*) the *upper* and *lower* sectors show opposite polarity (Figure 8c).

Besides, scanning pyroelectric microscopy was applied to three needle-shaped CNS crystals grown from toluene. The experiment consisted of placing them between two plate electrodes. By heating crystals locally, polarization develops and results in opposite excess charges on both electrodes. This induces a discharge current flowing through the outer circuit (for more details on the technique, see refs 20 and 13). Depending on the heated domain, the direction of the current is represented as either positive (red) or negative (blue). As shown in Figure 9, SPEM results confirmed the *bipolar* characteristic of the crystals and the expression of polarity along the *b* direction.

Finally, a recent re-investigation by X-ray diffraction of single crystals of CNS grown from toluene has shown a deviation from 50%:50% of *up* and *down* molecules. By refinement, a composition of 40%:60% with space group *P*1 was proposed. However, care has to be taken about the region of the crystal investigated: considering the structure as polar could be in contradiction with the bipolar state observed by SPEM. Therefore, we assume that the X-ray result corresponds to a single sector of the crystal or an overlap of sectors of different volumes. Further studies will focus on X-ray diffraction using cuts representing single sectors.

3.3 Validity of the Procedure. As shown previously, experimental data confirm the ability of the procedure to explain qualitatively the presence of growth-induced polarity in CNS crystals. From a quantitative point of view, the model represents fairly well the presence of polarity observed for growth sectors {011}. It seems however that the numerical GMMF model overestimates polarity, because a ratio of e.g., 25%:75% calculated for sectors is certainly too high for a crystal which by diffraction appears to be less polar.

Differences observed between experimental and computed results may arise due to *indirect* perturbations of growth-induced polarity as follows. (*i*) Even though dislocations or

geometrical twinning are not made responsible of the *formation* of polarity, they may *vary* the polar effects by perturbating the lattice. (*ii*) Considering the effects of solvents on polarity, solvent−solute interactions may influence the intensity of the polar effects. By solvating preferentially *A* or *D* groups at the interface, interaction energies between a docked molecule and its neighborhood at the surface are changed.

However, one has to highlight that polar effects for CNS crystals were observed whatever the crystallization method was (sublimation, melt, polar or nonpolar solvents, fast or slow growth rate) and that no polymorphism was suspected.

More generally, the three-step procedure is devoted to quantifying the *primary cause* of growth-induced polarity, which is a statistical deviation from a 50%:50% occupation.

From a technical point of view, utilization of this procedure requires consideration of the following several points. (*i*) Crystallographically distinct molecules in the unit-cell are considered elements of a Markov chain. As shown by CNS, molecules are related by symmetries in the bulk, but may become symmetry-independent on certain faces. (*ii*) Although extended to a GMMF model, layer-by-layer growth is not the most frequent growth mode of crystals. Therefore, a description by edge, kink, or even spiral or roughening growth would be more appropriate.[32] GMMF and Monte Carlo simulations show that the present description can be modified by taking into account an appropriate number of neighbors (effective coordination number), according to the type of surface growth mode.

Essential progress can be expected by using Monte Carlo methods, which have the advantage of giving a direct visualization of the vectors, as well as taking into account local correlations.

Conclusion

We developed a procedure to predict growth-induced polarity occurring in centrosymmetric crystals of dipolar molecules. The procedure can be described in three steps: (*i*) calculation of all the possible molecular interaction energies in the bulk, (*ii*) determination of the most important growing faces, and (*iii*) application of the generalized Markov mean-field (GMMF) model to the various faces composing the crystal.

The procedure has been applied with success to *trans*-4-chloro-4′-nitrostilbene. Significant effects of polarity for faces {011}, resulting in opposite polarity for $+b$ and $-b$ sectors of CNS crystals were predicted, a result confirmed by phase-sensitive second-harmonic microscopy and scanning pyroelectric microscopy experiments. Moreover, whatever the force field or set of charges used, the sign of X_{net} was negative, which indicates that surfaces {011} were composed of a majority of molecules pointing their *Cl* group toward the nutrient.

This example demonstrates that a single-component crystal can exhibit inhomogeneity in its packing, leading to the creation or modification of physical properties. Growth-induced polarity is thermodynamically driven and can be explained by the breaking of symmetries at the surface of

(32) Wüst, T.; Hulliger, J. To be submitted for publication.

the growing faces. A parallel can be drawn with the selective inclusion of impurities,[28] or the formation of polarity in centric solid solutions between polar and nonpolar molecules.[33]

The insertion of impurity with a different shape, or the 180° rotation of $A - \pi - D$ molecules with A and D having different volumes lead to an alteration of the lattice, a perturbation which can be in some extent observed and quantified by diffraction techniques.[34] However, when the "chemical defects" have similar volumes and shapes, their presence in the crystal may be difficult to investigate experimentally. In that case, a molecular modeling procedure[35] such as that developed here is a relatively straightforward alternative, as soon as the energy calculation methods are available for the type of compound studied.

(33) Wüst, T.; Gervais, C.; Hulliger, J. *Cryst. Growth Des.*, published online Sept. 14, http://dx.doi.org/10.1021/cg0342563..
(34) Bürgi, H. B. *Annu. Rev. Phys. Chem.* **2000**, *51*, 275−296.
(35) Galli, S.; Mercandelli. P.; Sironi, A. *J. Am. Chem. Soc.* **1999**, *121*, 3767−3772.

Note Added after ASAP Publication. Some of the *E* expressions in equation 3 contained errors in the version published ASAP December 10, 2004; the corrected version was published ASAP December 21, 2004.

Supporting Information Available: Influence of the cutoff distance on *tip-back* interaction energies, neighborhoods for families {011}, {100}, and {110}, influence of the force field and minimization on the calculated interaction energies, influence of the optimization of supercells with different ratios (*up*/*down*) on unit-cell parameters (PDF). This material is available free of charge via the Internet at http://pubs.acs.org.

CM0492033